On the Evaluation of Vorticity Using Cardiovascular Magnetic Resonance Velocity Measurements

J. Garcia
Québec Heart and Lung Institute,
Laval University,
Quebec City, QC G1V 0A6, Canada;
Laboratory of Cardiovascular Fluid Dynamics,
Concordia University,
Montréal QC H3G 1M8, Canada

E. Larose

P. Pibarot

Québec Heart and Lung Institute,
Laval University
Quebec City, QC G1V 0A6, Canada

L. Kadem[1]
Laboratory of Cardiovascular Fluid Dynamics,
Concordia University,
Montréal QC H3G 1M8, Canada
e-mail: kadem@encs.concordia.ca

Vorticity and vortical structures play a fundamental role affecting the evaluation of energetic aspects (mainly left ventricle work) of cardiovascular function. Vorticity can be derived from cardiovascular magnetic resonance (CMR) imaging velocity measurements. However, several numerical schemes can be used to evaluate the vorticity field. The main objective of this work is to assess different numerical schemes used to evaluate the vorticity field derived from CMR velocity measurements. We compared the vorticity field obtained using direct differentiation schemes (eight-point circulation and Chapra) and derivate differentiation schemes (Richardson 4 and compact Richardson 4*) from a theoretical velocity field and in vivo CMR velocity measurements. In all cases, the effect of artificial spatial resolution up-sampling and signal-to-noise ratio (SNR) on vorticity computation was evaluated. Theoretical and in vivo results showed that the eight-point circulation method underestimated vorticity. Up-sampling evaluation showed that the artificial improvement of spatial resolution had no effect on mean absolute vorticity estimation but it affected SNR for all methods. The Richardson 4* method and its compact version were the most accurate and stable methods for vorticity magnitude evaluation. Vorticity field determination using the eight-point circulation method, the most common method used in CMR, has reduced accuracy compared to other vorticity schemes. Richardson 4* and its compact version showed stable SNR using both theoretical and in vivo data.* [DOI: 10.1115/1.4025385]

Introduction

Vorticity and vortical structures play a fundamental role affecting the evaluation of energetic aspects of cardiovascular function. In cardiovascular flows, recirculation zones are usually detected by a visual inspection of the velocity field [1]. For a more accurate determination of vortical structures in the flow, a vorticity field has to be computed from a velocity field. A vorticity field also gives information regarding the magnitude of the shear layers present in the flow that may lead to thrombus formation and hemolysis [2].

In clinical practice, transthoracic Doppler echocardiography (TTE) is the most commonly used imaging technique to evaluate cardiovascular diseases. It has been demonstrated using color TTE that vortex formation and swirling flow in the left ventricle is highly related to dilated cardiomyopathy and/or ventricular altered geometry [3]. However, some technical limitations associated with TTE do not allow such analyses to be performed in all patients. In this case cardiovascular magnetic resonance (CMR) velocity measurements are a good option for flow visualization, measurement, and analysis in the majority of cardiac structures [1]. Detailed reviews on CMR and TTE vortex evaluation and flow analysis were recently performed [1,3]. The challenge is then to accurately characterize these flow structures and to link them to abnormal cardiovascular functions. There are several previous works aimed at understanding vortex formation induced by biological fluid transport [4], using vortex statistical approaches [5], or CMR vortex detection [3]. In such studies, accurate vorticity field quantification is of primary importance. However, several numerical schemes can be used to evaluate the vorticity field in a fluid flow. It is important to determine the accuracy of these different schemes to a more precise understanding of the link between the vorticity field in cardiac cavities and cardiovascular pathologies.

The objective of this study was to evaluate and to compare the most common vorticity schemes in the context of in vivo CMR velocity measurements.

Methods

Evaluation of the Vorticity Field in a Fluid Flow

Vorticity Schemes. Vorticity is closely related to the angular velocity of flow at a specific point and it is defined in two-dimensional Cartesian coordinates as follows:

$$\omega = \left(\frac{\partial V_y}{\partial x} - \frac{\partial V_x}{\partial y}\right)_{i,j} \tag{1}$$

where ω (1/s) is the vorticity and V is the velocity field for a location (i, j) (Fig. 1(*a*)).

Since velocity measurements by CMR are only available at specific points in the flow, a discrete scheme for vorticity determination has to then be used. The two most important standard schemes are: direct differentiation schemes and derivate differentiation schemes (Fig. 1(*b*)). Direct differentiation schemes are based on a short level of differential operators to approximate the gradient of a function based on a central point of differentiation. The complete vorticity field is then computed by shifting the region of interest along the velocity field. Among this category of schemes we selected a second-order eight-point circulation method and fourth-order Chapra method [6].

In the eight-point circulation method the central finite difference using circulation is calculated as the line integral of the dot product of the tangential velocity with the outward normal for a location (i, j)

$$\omega_z(i,j) = \frac{1}{\Delta}\left[-\frac{U_{i,j+1} - U_{i,j-1}}{2} + \frac{V_{i+1,j} - V_{i-1,j}}{2}\right] \tag{2}$$

where ω (1/s) is the vorticity, U and V are the velocity components in the x and y directions, and Δ is the spatial resolution. Using a second-order truncation error, the eight-point vorticity estimation scheme becomes

[1]Corresponding author.

Contributed by the Bioengineering Division of ASME for publication in the Journal of Biomechanical Engineering. Manuscript received April 2, 2012; final manuscript received June 15, 2012; accepted manuscript posted September 12, 2013; published online October 24, 2013. Assoc. Editor: Hai-Chao Han.

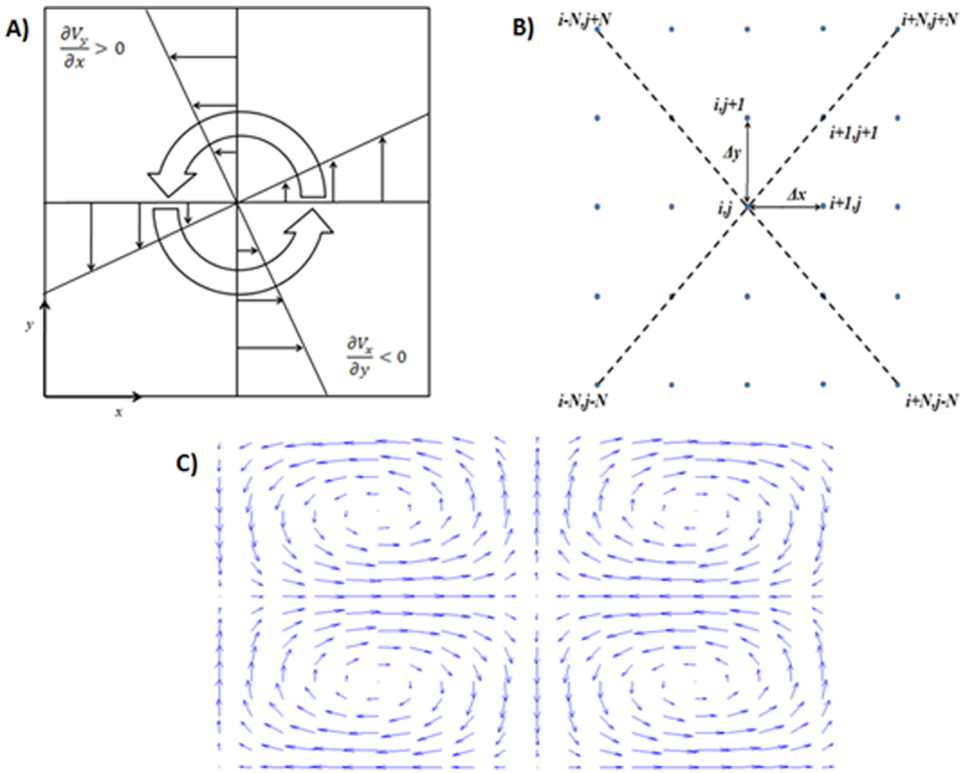

Fig. 1 Vorticity computation. (*a*) shows an example of vortical flow. (*b*) shows the vorticity computation using the finite differences. (*c*) shows the theoretical vortical cellular flow used to test vorticity schemes.

$$\omega_z(i,j) = \frac{1}{4\Delta}[(U_{i,j-1} - U_{i,j+1}) + (V_{i+1,j} - V_{i-1,j}) + 0.5(-U_{i+1,j+1} + V_{i+1,j+1} - U_{i-1,j+1} - V_{i-1,j+1} + U_{i-1,j-1} - V_{i-1,j-1} + U_{i+1,j-1} + V_{i-1,j-1})] \quad (3)$$

The fourth-order central difference approximation, named the Chapra method [7] is given by

$$\omega_z(i,j) = \frac{1}{\Delta}\left[-\frac{U_{i,j+2} - 8U_{i,j+1} + 8U_{i,j-1} - U_{i,j-2}}{12} + \frac{V_{i+2,j} - 8V_{i+1,j} + 8V_{i-1,j} - V_{i-2,j}}{12}\right] \quad (4)$$

Derivate differentiation schemes approximate the local gradients from velocity measurements. We evaluated the fourth-order Richardson extrapolation (R4*) [8] defined as

$$\frac{\partial U}{\partial x_i} = \frac{1}{A}\Sigma_{k=1,2,4,8} A_k \frac{U_{i+k}U_{i-k}}{2k\Delta x_i} \quad (5)$$

The fourth-order noise-minimizing R4* reduces the random error transmission by combining a range of second-order central difference schemes by selecting an optimized set of coefficients (see Table 2 from Ref. [8]). A compact version of the Richardson extrapolation scheme (CR4*) is also evaluated and it is defined as

$$\frac{\partial U}{\partial x_i} = \frac{1}{A}\Sigma_{k=1,2,4,8} A_k U'_{i,k-grid} \quad (6)$$

where $U'_{i,k\text{-}grid}$ is the implicitly computed derivative from the compact scheme for k-grid spacing. The CR4* reduces the random error transmission by increasing the order of truncation error and an optimized set of coefficients improving the cost of noise amplification (see Table 3 from Ref. [8]).

Theoretical Reference Vorticity Field. Given the absence of a physical standard reference for vorticity estimation, we considered as reference the theoretical velocity field represented by six different vortical cellular flows [9]:

$$u = V_{max}\cos\left(\frac{xN_x\pi}{L_x} + \frac{\pi}{2}\right)\cos\left(\frac{yN_y\pi}{L_y}\right) \quad (7)$$

$$v = V_{max}\sin\left(\frac{xN_x\pi}{L_x} + \frac{\pi}{2}\right)\sin\left(\frac{yN_y\pi}{L_y}\right)$$

where u and v are the velocity components in x and y directions, respectively. L_x and L_y are the sizes of the field-of-view (here: 400×400 pixel) in the x and y directions, $N_{xy} = 2$ are the number of cores and $V_{\max}$ (0.5–5 m/s) is the maximum velocity in the cell map (Fig. 1(*c*)). This theoretical model has the advantage of simulating multiple vortex cores, a configuration often found in heart cavities.

Several tests were performed to alter the velocity field obtained by Eq. (7). The resulting vorticity fields determined using the four above schemes were compared to the theoretical derived vorticity field. In this study, the following tests were performed: (1) the effect of artificial up-sampling on vorticity computation was evaluated by increasing 2–4 times the spatial resolution from 2 mm to 0.5 mm, as is expected in in vivo settings, and the impact of up-sampling was evaluated in terms of signal-to-noise ratio (SNR); and (2) the effect of the presence of noise in the velocity field on vorticity computation was evaluated by introducing a Gaussian noise on the u and v velocity components [10]. Image up-sampling was artificially improved using a bicubic averaged interpolation.

In Vivo Evaluation of Vorticity Field

Patient Population. One healthy subject and three patients with aortic valve stenosis (AS) were included in this study. The study

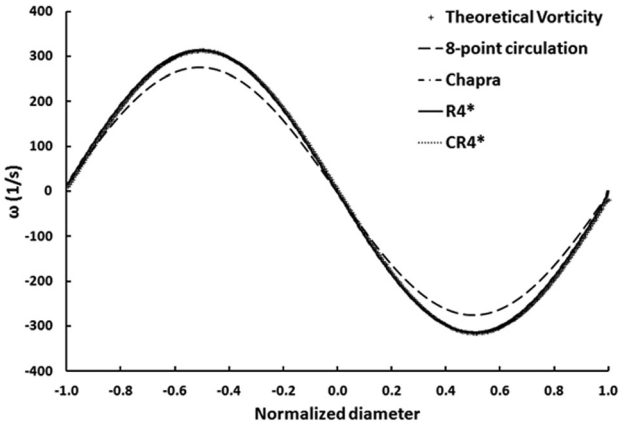

Fig. 2 Vorticity computed for V_{max} of 5 m/s. Vorticity profile, as determined by each method, corresponding to the central line of the top cells in Fig. 1(*c*).

was approved by the Institutional Review Board and all patients provided written informed consent. An exclusion criterion was major restrictions to undergo a CMR scan. Effective orifice area (EOA) was determined using continuity equation [11,12].

Cardiovascular Magnetic Resonance. CMR studies were performed with a 1.5 T Philips Achieva scanner operating release 2.6 level 3 and dedicated phased-array cardiac coil during successive end-expiratory breath holds (Philips Healthcare, Best, The Netherlands). Cine imaging of cardiac function was performed by steady state free precession (SSFP) technique at 30 phases per cardiac cycle (by vectorcardiographic gating) in 8–14 parallel short-axis and two-chamber, four-chamber, and two orthogonal left ventricle outflow tract (LVOT) planes (8 mm thickness, 0 mm gap). Typical parameters included TR/TE of 3.4/1.2 ms, flip angle 40 deg, NEX of 1, yielding in-plane spatial resolution of 1.6×2 mm. In addition, through-plane phase-contrast imaging was performed in the LVOT and in the ascending aorta [12]. Flow velocity measurements were performed in the dominant direction of the flow in order to compute effective orifice area by continuity equation. Two orthogonal LVOT planes were also acquired in the three directions of the flow. CMR imaging parameters consisted of: TR/TE of 4.60–4.92/2.76–3.05 ms, flip angle 15 deg, 24 phases, pixel spacing 1.32–2.07 mm, slice thickness 10 mm, and acquisition matrix of 256×208. For each patient CMR encoding velocity was adjusted to optimally define velocity resolution and avoid velocity aliasing ($V_{enc} = 1.25 \times V_{max}$). Total scan time was 15 min. Background noise filtering was performed for all sets of images. A custom-made research application was developed using MATLAB software (Mathworks, Natick, MA) to process and analyze both theoretical and in vivo images.

Table 1 Patients' characteristics The table shows the mean ± SD or number of patients and percentage

Age (years)	56 ± 17
Male gender *n* (%)	3 (60)
Heart rate (bpm)	65 ± 12
Weight (kg)	80 ± 11
Height (cm)	167 ± 11
Body surface area (m^2)	1.93 ± 0.2
Body mass index (kg/m^2)	28 ± 1
Valve morphology	
Tricuspid *n* (%)	3 (75)
Bicuspid *n* (%)	1 (25)

Results

Theoretical Vortical Cellular Flows. Six simulated vortical cellular flows were used to theoretically evaluate the four proposed methods to estimate vorticity field. Figure 2 shows the comparison between the vorticity profiles estimated using all the methods and the theoretically predicted vorticity. It clearly appears that all methods accurately evaluate vorticity distribution compared to theoretical predictions, except for the eight-point circulation method, which underestimates the vorticity magnitude. It should be noted, however, that the eight-point circulation method led to accurate results up to V_{max} around 2 m/s (Fig. 3(*a*)).

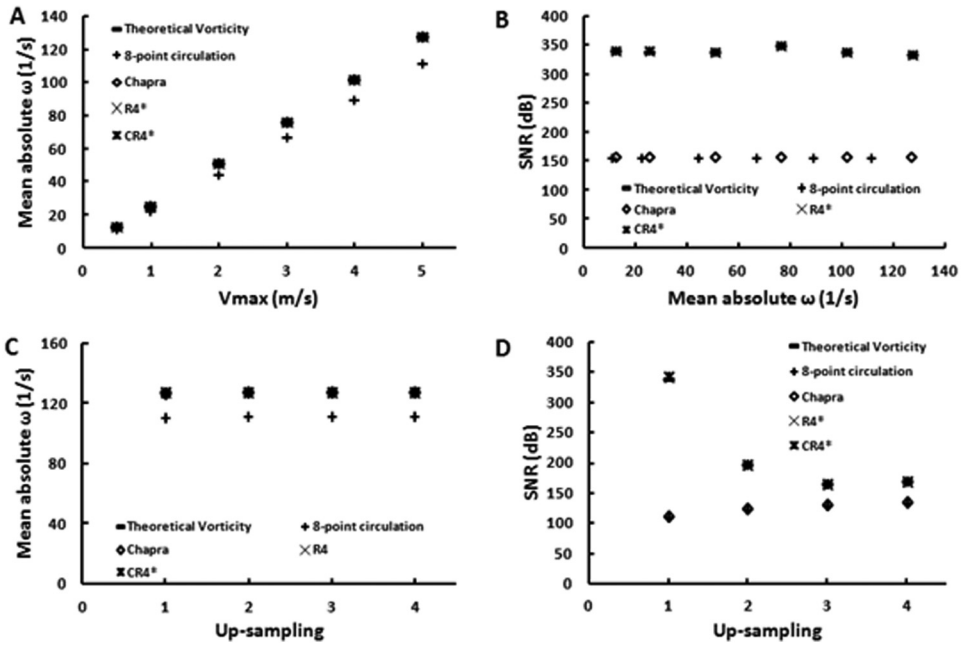

Fig. 3 Theoretical comparison of vorticity schemes and up-sampling effect. (*a*) shows the mean absolute vorticity computed using vorticity schemes from the theoretical velocity field. (*b*) shows the evaluation of signal-to-noise ratio (SNR). (*c*) shows the effect of image up-sampling on vorticity computation and (*d*) on the evaluation of SNR.

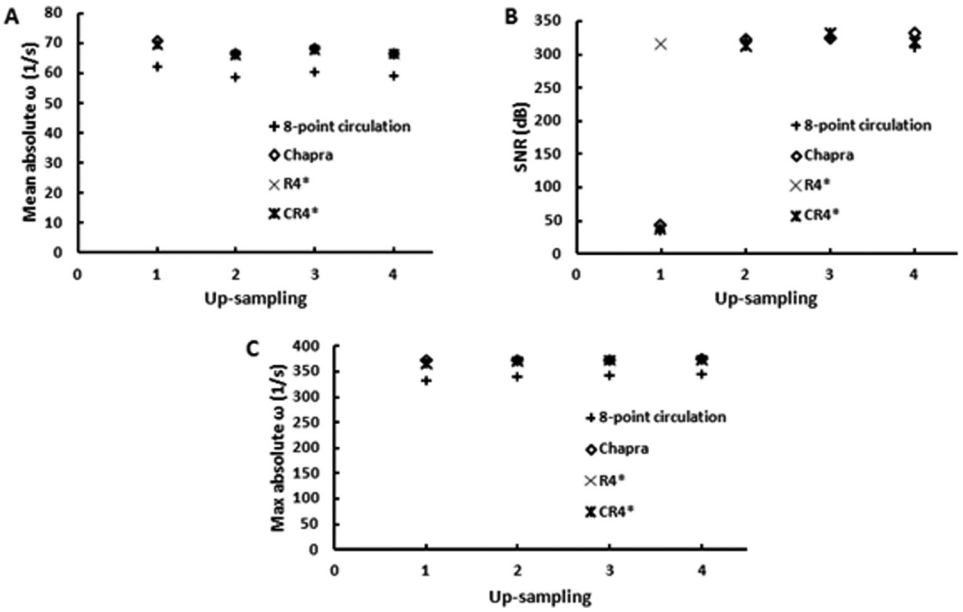

Fig. 4 Up-sampling evaluation of vorticity schemes using velocity map from a patient with severe aortic stenosis at peak systole. (*a*) shows the mean absolute vorticity computed using vorticity schemes. (*b*) shows the effect of image up-sampling on SNR. (*c*) shows the maximum absolute vorticity using vorticity schemes.

Effect of Gaussian Noise. Adding a Gaussian noise to the velocity field had a significant impact on signal-to-noise ratio (SNR) of direct differentiation schemes: eight-point circulation method and Chapra method (Fig. 3(*b*)). Derivate differentiation schemes (R4* and CR4*) had a significantly higher SNR (340 dB for both R4* and CR4*).

Effect of Artificial Up-Sampling. The effect of artificial up-sampling on the evaluation of vorticity field using the proposed schemes is shown in Figs. 3(*c*) and 3(*d*). It appears that artificial up-sampling does not have a significant effect on the computed absolute mean vorticity. However, the eight-point circulation method underestimated systematically the absolute mean vorticity (Fig. 3(*c*)). Regarding SNR magnitude, although, it decreased as a function of artificial up-sampling, SNR for R4* and CR4* remained always higher than those obtained using the eight-point circulation method and Chapra (Fig. 3(*d*)).

In Vivo Evaluation. Vorticity field computation was performed in vivo on one healthy subject and three patients (men, age 56 ± 17 years). Patients' characteristics are given in Table 1. The effective orifice area (EOA) computed by CMR using continuity equation for patients were: healthy ($EOA = 3.4\,\text{cm}^2$), mild ($EOA = 1.73\,\text{cm}^2$), moderate ($EOA = 1.13\,\text{cm}^2$), and severe ($EOA = 0.95\,\text{cm}^2$). Vorticity magnitude was higher in the presence of severe aortic stenosis than in the healthy aortic valve (mean absolute vorticity $= 66 \pm 3$ 1/s and 11 ± 1 1/s, $p < 0.001$,

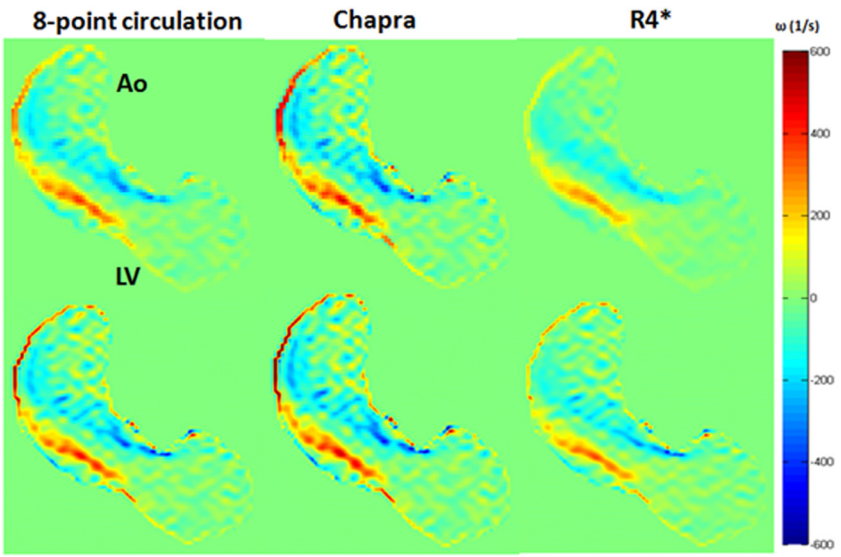

Fig. 5 Effect of image up-sampling on vorticity computation *in vivo*. First raw: low resolution vorticity magnitude. Second raw: high resolution (four times original) vorticity magnitude. Vorticity magnitude was computed from velocity measurements in a patient with severe aortic stenosis at peak systole phase. Ao is the ascending aorta; LV is the left ventricle.

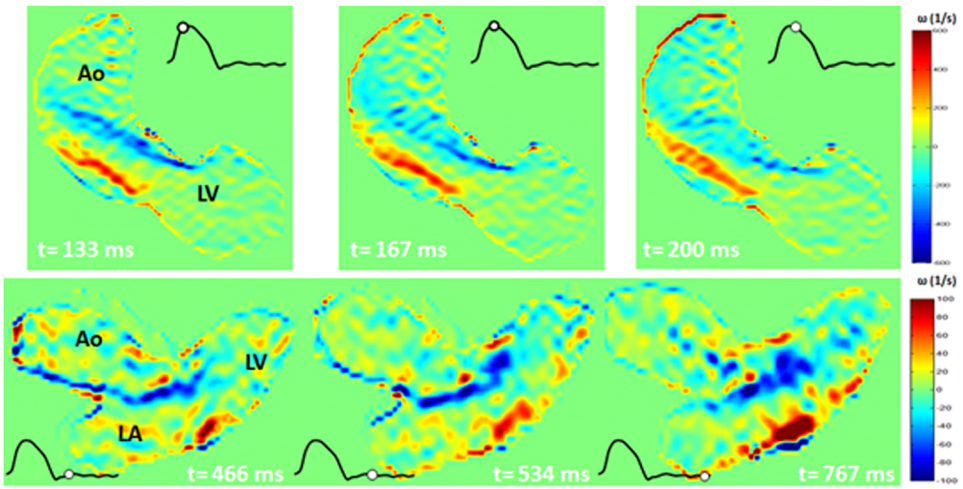

Fig. 6 Vorticity magnitude computation in the ascending aorta and left ventricle at different instants of cardiac cycle using R4*. Top panels show the ascending aorta region in a patient with severe aortic stenosis, whereas the bottom panels show the mitral valve region for the same patient. Ao is the ascending aorta; LV is the left ventricle; LA is the left atrium. Black line is the flow plot over cardiac cycle.

respectively). Mild and moderate aortic stenosis showed similar magnitudes (mean absolute vorticity = 54 ± 3 1/s and 56 ± 3 1/s, respectively).

First, we evaluated the effect of an artificial up-sampling on SNR for the case of severe aortic stenosis. The SNR for R4* remained elevated regardless of the spatial resolution. For all other methods, SNR started increasing only after doubling the spatial resolution (Fig. 4(*b*)). The mean and maximum absolute vorticity magnitudes were computed and remained relatively constant with all methods using the same set of images. The eight-point circulation method underestimated systematically the vorticity magnitude as expected from the theoretical vorticity field analysis (Figs. 4(*a*) and 4(*c*)). Figure 5 shows a comparison of the vorticity magnitude using actual CMR spatial resolution and after four time artificial improvement. The in vivo vorticity field of aortic valve and mitral valve in a patient with severe aortic stenosis during cardiac cycle is displayed in Fig. 6. A zoom of streamlines vortex cores in the left atrium of a patient with moderate aortic stenosis using high spatial resolution and R4* at different systolic times is displayed in Fig. 7. Of interest, the left atrium vorticity magnitude is significantly lower than the one observed in the aortic valve and closer to the one in the mitral valve.

Discussion

CMR measurements provide effective, noninvasive, qualitative, and quantitative characterization of blood flow compared with traditional TTE. Flow velocity measurements with CMR are used for streamline visualizations, flow volume and/or pressure gradient quantification, evaluation of wall shear stress, oscillatory shear index, and kinetic energy [1]. CMR can also evaluate the vorticity field, an essential parameter for understanding blood flow dynamics and its link to the appearance of cardiovascular diseases [3,5]. In this study we evaluated, theoretically and with in vivo CMR velocity images, the most commonly used schemes to estimate vorticity magnitude in experimental fluid mechanics.

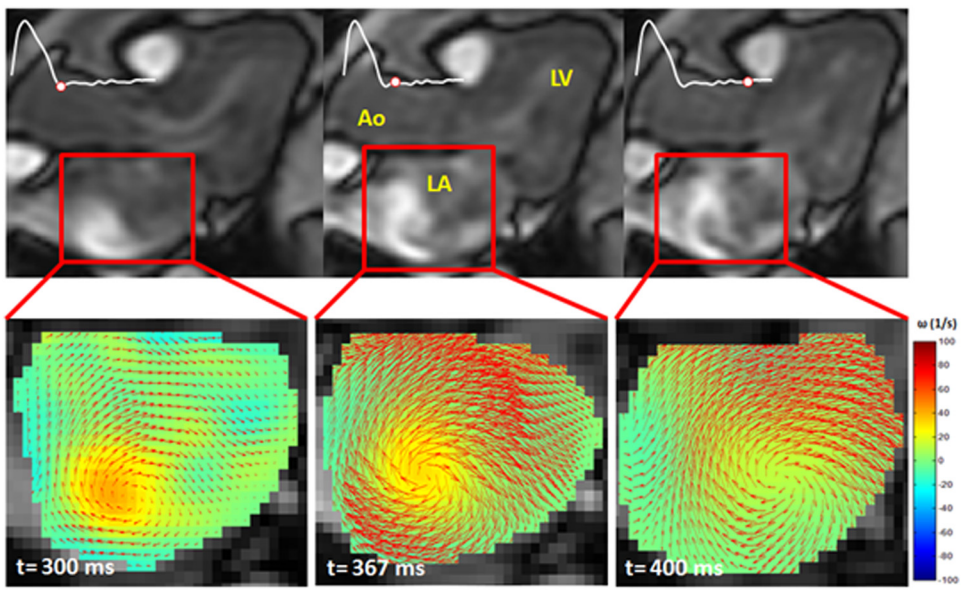

Fig. 7 Vorticity magnitude computation in the left atrium at three different instants of cardiac cycle using R4*. Ao is the ascending aorta; LV is the left ventricle; LA is the left atrium. White line is the flow plot over time.

Theoretical and in vivo data showed that an eight-point circulation method underestimates the vorticity magnitude and that the most stable scheme with and without artificial up-sampling was R4*. These are important results given that the eight-point circulation method is currently the method of choice when determining the vorticity field from velocity measurements [6]. The results obtained in this study are consistent with those of Etebari and Vlachos [8]. The Chapra second-order scheme led to relatively similar results in terms of vorticity magnitude, but SNR was significantly lower compared to R4* and CR4*. These differences can be explained by the truncation error associated with each scheme, the spatial resolution, and the potential amplification of the error close to wall vessels. Although all methods seem to be capable of qualitatively capturing vortical structures and shear layers existing in the flow field (shear layers are strongly related to hemolysis in AS patients [13]) quantitative differences exist between the methods. These differences can be amplified when trying to evaluate important effects like the dissipation effects in the flow (enstrophy computation).

Conclusions

The vorticity field can be determined using CMR. However, its accuracy depends on the numerical scheme used to derive vorticity from the velocity field. Using and eight-point circulation method underestimates vorticity magnitude. Richardson 4* and Compact Richardson 4* interpolation led to more accurate results and higher SNR both using a theoretical velocity field and in vivo data.

Acknowledgment

This work was supported by an NSERC grant (343165-07), the Canada Research Chair in Valvular Heart Diseases, CIHR (Canada), and CONACyT (Mexico).

References

[1] Markl, M., Kilner, P. J., and Ebbers, T., 2011, "Comprehensive 4D Velocity Mapping of the Heart and Great Vessels by Cardiovascular Magnetic Resonance," J. Cardiovasc. Magn. Reson., **13**, p. 7.
[2] Bluestein, D., Chandran, K. B., and Manning, K. B., 2010, "Towards Non-Thrombogenic Performance of Blood Recirculating Devices," Ann. Biomed. Eng., **38**(3), pp. 1236–1256.
[3] Sengupta, P. P., Pedrizzetti, G., Kilner, P. J., Kheradvar, A., Ebbers, T., Tonti, G., Fraser, A. G., and Narula, J., 2012, "Emerging Trends in CV Flow Visualization," JACC Cardiovasc. Imag., **5**(3), pp. 305–316.
[4] Dabiri, J. O., and Gharib, M., 2005, "The Role of Optimal Vortex Formation in Biological Fluid Transport," Proc. Biol. Sci., **272**(1572), pp. 1557–1560.
[5] Gharib, M., Rambod, E., Kheradvar, A., and Sahn, D., 2006, "Optimal Vortex Formation as an Index of Cardiac Health," Proc. Natl. Acad. Sc. USA, **103**(16), pp. 6305–6308.
[6] Luff, J. D., Drouillard, T., Rompage, A. M., Linne, M. A., and Hertzberg, J. R., 1999, "Experimental Uncertainties Associated With Particle Image Velocimetry (PIV) Based Vorticity Algorithms," Experiments Fluids, **26**, pp. 36–54.
[7] Chapra, S., 1998, *Numerical Methods for Engineers*, 2nd ed. McGraw-Hill Inc, New York, p. 529.
[8] Etebari, A., and Vlachos, P. P., 2005, "Improvements on the Accuracy of Derivative Estimation From DPIV Velocity Measurements," Experiments Fluids, **39**, pp. 1040–1050.
[9] Shinneeb, A.-M., Bugg, J. D., and Balachandar, R., 2004, "Variable Threshold Outlier Identification in PIV Data," Meas. Sci. Technol., **15**(9), pp. 1722–1732.
[10] Gao, J. H., and Gore, J. O., 1991, "Turbulent Flow Effects on NMR Imaging: Measurement of Turbulent Intensity," Med. Phys., **18**(5), pp. 1045–1051.
[11] Bonow, R. O., Carabello, B., Chatterjee, K., de Leon, A., Faxon, D., Freed, M., Gaasch, W., Lytle, B., Nishimura, R., O'Gara, P., O'Rourke, R., Otto, C., Shah, P., and Shanewise, J., 2008, "2008 Focused Update Incorporated Into the ACC/AHA 2006 Guidelines for the Management of Patients With Valvular Heart Disease: A Report of the American College of Cardiology/American Heart Association Task Force on Practice Guidelines," Circulation, **118**(15), pp. e523–e661.
[12] Garcia, J., Kadem, L., Larose, E., Clavel, M.-A., and Pibarot, P., 2011, "Comparison Between Cardiovascular Magnetic Resonance and Transthoracic Doppler Echocardiography for the Estimation of Effective Orifice Area in Aortic Stenosis," J. Cardiovasc. Magn. Reson., **13**, p. 25.
[13] Vincentelli, A., Susen, S., Le Tourneau, T., Six, I., Fabre, O., Juthier, F., Bauters, A., Decoene, C., Goudemand, J., Prat, A., and Jude, B., 2003, "Acquired von Willebrand Syndrome in Aortic Stenosis," N. Engl. J. Med., **349**(4), pp. 343–349.